

PACS numbers: 61.72.Uj, 71.55.Eq, 78.40.Fy, 82.30.Lp

**TITANIUM-MANGANESE OXIDES.  
OPTICAL AND PHOTOCATALYTIC PROPERTIES**

**L. Kernazhitsky<sup>1</sup>, V. Shymanovska<sup>1</sup>, T. Gavrilko<sup>1</sup>, G. Puchkowska<sup>1</sup>, V. Naumov<sup>1</sup>,  
T. Khalyavka<sup>2</sup>, V. Kshnyakin<sup>3</sup>, V. Chernyak<sup>4</sup>, J. Baran<sup>5</sup>**

<sup>1</sup> Institute of Physics, National Academy of Sciences of Ukraine,  
46, Nauki Prosp., 03028, Kiev, Ukraine  
E-mail: [puchkov@iop.kiev.ua](mailto:puchkov@iop.kiev.ua)

<sup>2</sup> Institute for Sorption and Problems of Endoecology, NAS of Ukraine,  
13, Gen. Naumov Str., 03164, Kiev, Ukraine

<sup>3</sup> Sumy State University,  
2, Rimsky-Korsakov Str., 40007, Sumy, Ukraine

<sup>4</sup> Taras Shevchenko National University,  
2/5, Acad. Glushkov Prosp., 03122, Kiev, Ukraine

<sup>5</sup> Institute of Low Temperature and Structure Research, PAS,  
50-950, Wroclaw, Poland

*Nanocrystalline titanium-manganese mixed oxides (TMO) with the Mn content of 13-16 % at. were first synthesized by manganese hydroxide precipitation on anatase or rutile particles. The structure, morphology and chemical composition of the samples were characterized using XRD and XRF methods showing that the synthesized mixed oxides are the polydisperse materials of different phase composition containing TiO<sub>2</sub>, Mn<sub>2</sub>O<sub>3</sub> and MnTiO<sub>3</sub>. The phase transformations and structure defects of the prepared compounds were characterized by FTIR, FT-FIR, FT-Raman spectroscopies. UV-VIS absorption spectra were investigated in 2,4-6,0 eV region, and it was revealed that the presence of manganese oxides results in absorption increase and significant red shift of the TMO absorption edge in comparison with pure TiO<sub>2</sub>. Photocatalytic activity of pure TiO<sub>2</sub>, Mn<sup>2+</sup>-doped TiO<sub>2</sub> and TMO during the photocatalytic decomposition of the safranine dye under UV irradiation was studied. A great improvement of photocatalytic activity is registered for Mn<sup>2+</sup>-doped TiO<sub>2</sub> (anatase and rutile), and rutile-based TMO sample.*

**Keywords:** TITANIUM-MANGANESE OXIDES, OPTICAL PROPERTIES, PHOTOCATALYSIS, SAFRANINE.

*(Received 28 May 2010, in final form 29 June 2010)*

## 1. INTRODUCTION

Prospects of wide practical application of TiO<sub>2</sub> wide gap semiconductor as an effective solar energy converter and photocatalyzer are somewhat restricted due to essential width of its band gap (which is 3 eV for rutile and 3,2 eV for anatase) that leads to necessity of application of ultra-violet radiation. To improve the photoactivity and extend the working range of this material, TiO<sub>2</sub> is doped by different elements, such as, cations of transition metals, sulfur, nitrogen, etc [1-3]. Under action of impurities, change of equilibrium

electron and hole concentration occurs and shift of optical absorption band to visible spectral region is observed. Significant amount of publications was devoted to efforts of influence on the physical, chemical, and optical properties of  $\text{TiO}_2$  by doping it with other oxides [4-6]. Properties of such complex oxides can be changed depending on the synthesis technique and their chemical composition. In particular, mixed  $\text{TiO}_2/\text{MnO}_x$  oxides based on manganese oxides of different composition are of a great interest. This is conditioned by high solubility of manganese in  $\text{TiO}_2$  that, as it is expected, can lead to appearance of interesting optical and photocatalytic properties.

In our previous paper [7] the UV absorption spectra of pure rutile and rutile with the surface modified by cations of transition metals (Cr, Cu, Co, and Fe) were investigated nearby the fundamental absorption edge. Obtained data was compared with the activity of titanium dioxide in the reaction of photocatalytic decomposition of safranine dye under UV radiation.

In the given work we present the investigation results of the optical and photocatalytic properties of firstly synthesized titanium-manganese mixed oxides (TMO) with different Mn content (8-16% at). TMO samples were synthesized by chemical precipitation of manganese hydroxide on the polycrystalline particles of pure  $\text{TiO}_2$  (rutile or anatase) with further thermal treatment at the temperatures of 300, 850, 900 and 1000 °C. Pure samples of rutile and anatase, as well as rutile and anatase modified by  $\text{Mn}^{2+}$  were synthesized for the comparison. Morphology, structure, optical and physical properties of the obtained samples were studied by the X-ray diffraction (XRD) and X-ray fluorescence (XRF) methods, optical absorption spectroscopy in visible and UV ranges and by the IR absorption spectroscopy and combinational light dispersion (CLD) with the Fourier transformation. Photo-catalytic activity of the samples was estimated using the photodegradation reaction of safranine in aqueous solution (which was the model one) under UV radiation.

## 2. MATERIALS AND INVESTIGATION METHODS

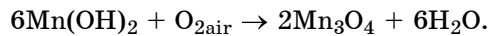
### 2.1 Materials

For the investigation we have synthesized polydisperse samples of pure nanocrystalline  $\text{TiO}_2$  with anatase (An) and rutile (R) structure. Samples were obtained by thermal hydrolysis of  $\text{TiCl}_4$  muriatic solutions with further thermal treatment at 300 °C [8]. To prepare TMO, the calculated amount 0,1 M of  $\text{MnCl}_2 \cdot 4\text{H}_2\text{O}$  aqueous solution was added to the recently synthesized pure  $\text{TiO}_2$  at room temperature with continuous agitation during an hour. Then 0,5 M aqueous solution of ammonium bicarbonate ( $\text{NH}_4\text{HCO}_3$ ) was added to the suspension up to pH = 8,7-9,0. The reaction resulted in the manganese hydroxide

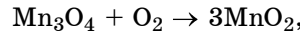


TMO samples were prepared based on nanocrystalline particles both of anatase (TMO-1) and rutile (TMO-2, TMO-3). Obtained suspension was filtered, washed by distilled water and dried at 120°C. Then sediment was thoroughly washed by water to obtain a complete absence of chlorine ions in filtrate. After that sediment was fried in the air at different temperatures: 300 °C (4 hours), 850 °C (2 hours), 900 °C (2 hours) and 1000 °C (2 hours).

Manganese oxides of different composition can be formed as a result of air frying of manganese hydroxide:



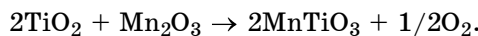
$\text{Mn}_3\text{O}_4$  is oxidized to  $\text{MnO}_2$  (polianite) during further thermal treatment in the presence of oxygen, i.e.,



and at the temperatures higher than 500 °C  $\text{Mn}_2\text{O}_3$  (braunite) appears:



While frying the mixture of titanium and manganese oxides at the temperatures higher than 900 °C, the following solid-phase reaction of  $\text{MnTiO}_3$  generation can take place:



For comparison we have prepared two samples of  $\text{TiO}_2$  with the surface modified by the method of  $\text{Mn}^{2+}$  adsorption on surface of anatase particles. Adsorption was performed from diluted aqueous solutions  $\text{MnCl}_2 \cdot 4\text{H}_2\text{O}$  and resulted in achievement of the sorption equilibrium (24 hours). Then samples were filtered and fried at 300 °C (An/Mn) or 900 °C (R/Mn).

## 2.2 Experimental techniques

Phase and chemical composition of the obtained samples was investigated by the XRD methods using diffractometer DRON-2 with  $\text{CuK}\alpha$  ( $\lambda = 0,154$  nm) radiation. Chemical composition of the samples was studied using the XRF analyzer with XNAT-Control add-on. Specific surface ( $S_{\text{BET}}$ ) of the samples was determined by the nitrogen adsorption using BET method. To study the adsorption spectra in IR, UV and visible ranges we have prepared the following samples: 1 mg of  $\text{TiO}_2$  or TMO was mixed with 150 mg of dry KBr in agate mortar with further pressing under 2 atm to transparent discs.

IR absorption spectra in the middle (4000-400  $\text{cm}^{-1}$ ) and the long-range (100-400  $\text{cm}^{-1}$ ) ranges were obtained using IR spectrometer with Fourier transformation IFS-88 of Bruker Comp. with spectral resolution of 2  $\text{cm}^{-1}$ . To obtain the high-quality spectra, we used the averaging over 64 scans of each spectrum. Accuracy of the spectra reconstruction through wave numbers was 0,5  $\text{cm}^{-1}$ , measuring accuracy of the absorption band intensity was 10%. All spectra were registered in the atmosphere of dry air at room temperature. CLD spectra of powder samples were measured in the spectral range of 80-4000  $\text{cm}^{-1}$  using FRA-106 add-on to the Bruker spectrometer IFS-88. To excite the CLD spectra we used Nd: YAG laser with  $\lambda_{ex} = 1,06 \mu\text{m}$  and the power of 300 mW. Spectra were registered in the backscattering geometry with spectral resolution of 2  $\text{cm}^{-1}$  and 32 scans.

Optical absorption spectra of the samples in the spectral region of 250-450 nm were studied using the standard deuterium lamp and portable PC operating based on CCD of multichannel optical analyzer SL40 (diffraction grating consists of 600 grooves per 1 mm, glitter is 350 nm, 3648-pixel linear sensor TCD1304AP, spectral resolution is 0,3 nm).

### 2.3 Photocatalytic decomposition of safranine

Photocatalytic activity of the synthesized materials was investigated in the reaction of safranine photodecomposition in aqueous solution. The reaction was carried out in quartz reactor at room temperature using the standard mercury lamp PRK-1000 (power is 1000 W,  $\lambda = 254$  nm). Reactor was 1 cm far from the lamp. The solution volume in reactor was 50 ml, initial dye concentration was 0,3 g/l, catalyst concentration ( $\text{TiO}_2$  or TMO) was 2 g/l, pH = 7. Suspension was mixed using magnetic mixer (rotational velocity is 120 revo/min) during the total time of irradiation. To control changes of a dye concentration, samples of the reaction mixture were taken through certain time intervals. Solid fraction was filtered out using centrifuge (8000 revo), and using spectrophotometer Specord-20 UV-VIS the safranine concentration in solution was determined.

## 3. RESULTS AND DISCUSSION

### 3.1 X-ray diffraction (XRD) analysis

Characteristics of the synthesized TMO and  $\text{TiO}_2$  samples are represented in Table 1. In accordance with the XRD analysis, the synthesized TMO samples are the polydisperse nanocrystalline powders, which are different by the phase composition. Thus, it was established that TMO-1 fried at 850 °C contains mixture of anatase, rutile, and  $\text{Mn}_2\text{O}_3$ . At the same time,  $\text{MnTiO}_3$  phase is present in TMO-2 and TMO-3 samples treated at higher temperatures (900 and 1000 °C). It is known that the crystallite size in polydisperse materials depends on the synthesis method and treatment temperature. Crystallite size in TMO samples was determined using the broadening of the X-ray diffraction maximums according to the Scherrer equation. It was revealed that the crystallite sizes of  $\text{TiO}_2$ ,  $\text{Mn}_2\text{O}_3$  and  $\text{MnTiO}_3$  are 52-120, 36-45, and 33-40 nm, respectively.

**Table 1 – Chemical composition and sample characteristic**

Sample	T, °C	Mn content, % at.*	Phase composition, % wt.**	Crystallite size, nm ( $D_{hkl}$ )
Pure $\text{TiO}_2$				
An	300	0	anatase	100 13,3 (101)
R	300	0	rutile	100 20,8 (110)
$\text{Mn}^{2+}$ adsorption on $\text{TiO}_2$				
An/Mn	300	1,0	anatase	100 15,4 (101)
R/Mn	900	1,0	anatase rutile	10,2 89,8 70,8 (101) 40,3 (110)
Precipitation of manganese hydroxide on anatase				
TMO-1	850	13,4	anatase Rutile $\text{Mn}_2\text{O}_3$	54,6 35,6 9,7 42,2 (101) 51,7 (110) 44,8 (222)
Precipitation of manganese hydroxide on rutile				
TMO-2	900	15,6	Rutile $\text{Mn}_2\text{O}_3$ $\text{MnTiO}_3$	85,7 12,1 2,2 120,8 (110) 36,0 (222) 32,6 (104)
TMO-3	1000	13,4	Rutile $\text{MnTiO}_3$	86,0 14,0 62,6 (110) 39,9 (104)

\* – the XRF data, \*\* – the XRD data

XRD analysis shows that An/Mn sample (synthesized based on anatase and thermally treated at 300 °C during 8 hours) consists of only one phase – anatase, while R/Mn sample obtained by An/Mn frying at 900 °C during 2 hours, also contains about 10% of residual anatase. In contrast to pure anatase, which after frying at 850 °C during 2 hours is completely transformed to rutile, TMO-1 sample after thermal treatment at 850 °C contains about 54,6% of anatase. These facts imply about significant influence of Mn ions on suppression of the anatase phase transformation to rutile.

### 3.2 IR spectroscopy

IR spectroscopy is the source of important information about the chemical composition and structure of the amorphous and crystalline materials. Also this method allows to find out the nature of active centers on the surface of oxides. IR absorption spectra of An/Mn, R/Mn, and TMO samples in the spectral range of 100-1000 cm<sup>-1</sup> at room temperature are represented in Fig. 1. Absorption bands observed in this region can be ascribed to the excitations of Ti-O, Ti-O-Ti, Mn-O, Mn-O-Mn and Mn-O-Ti bindings and to the vibrational modes of crystalline grating.

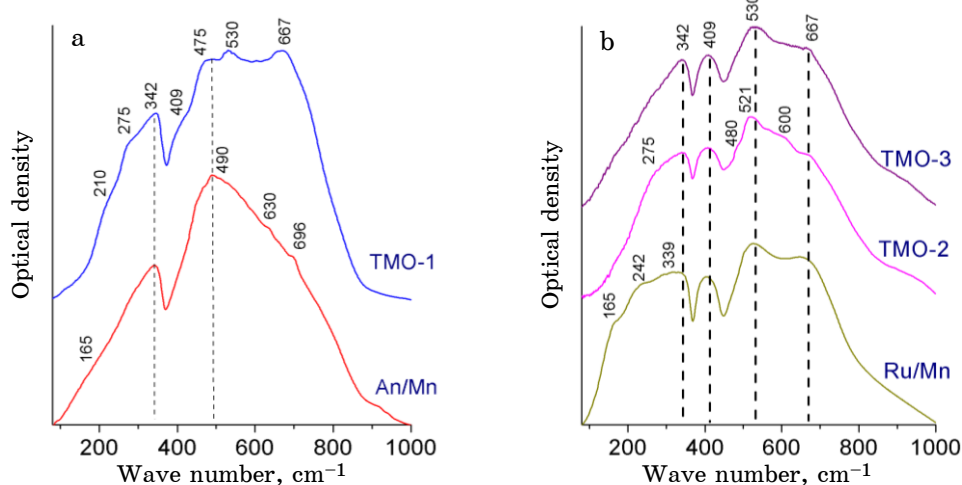


*Fig. 1 – IR absorption spectra of TiO<sub>2</sub> and TMO samples: a) An/Mn and TMO-1; b) R/Mn, TMO-2 and TMO-3*

As seen from Fig. 1a, An/Mn sample (100% anatase, 300 °C) has two main wide absorption bands with the maximums of 342 and 490 cm<sup>-1</sup>. We also observed some weak supplementary bands at 165, 242, 630, and 696 cm<sup>-1</sup>. According to [9], anatase monocrystal has three IR active modes ( $A_{2u} + 2E_u$ ) with corresponding absorption bands, which belong to TO(LO) phonons and are observed at 170 (900), 180 (360) and 420 (840) cm<sup>-1</sup>. Supplementary modes in the IR spectra of anatase (165 and 630 cm<sup>-1</sup>) can be ascribed to the excitations with oxygen vacancies on the surface of nanocrystalline particles and Ti<sup>3+</sup> cations, which are present in titanium dioxide at oxygen shortage.

4 IR active modes ( $A_{2u} + 3E_u$ ) with corresponding TO(LO) excitations at 160 (805), 180 (360), 376 (445) and 495 (780) cm<sup>-1</sup> are observed in the IR

absorption spectra of crystalline rutile [10]. All these main absorption bands were observed in the IR spectra of R/Mn sample (Fig. 1b), which after frying at 900 °C contains about 10% wt of anatase. Bands at 339, 407, 530 and 667 cm<sup>-1</sup> can be ascribed to the Ti-O excitations. Two bands at 165 and 242 cm<sup>-1</sup> are conditioned by Ti-O excitations of anatase.

Crystalline Mn<sub>2</sub>O<sub>3</sub> has three main IR absorption bands at 521, 575 and 664 cm<sup>-1</sup> [11]. It was shown that the IR absorption spectrum of nanocrystalline Mn<sub>2</sub>O<sub>3</sub> is shifted as a whole to the high-frequency region and its shape depends on the size of nanoparticles. The corresponding absorption bands were ascribed to the symmetric (506 cm<sup>-1</sup>) and asymmetric (603 cm<sup>-1</sup>) valence and deformation (404 cm<sup>-1</sup>) excitations of Mn-O-Mn in separate “molecular” fragments.

IR spectra of bulk MnTiO<sub>3</sub> are characterized by the presence of two intensive absorption bands at 533 and 620 cm<sup>-1</sup>, which correspond to Mn-O-Ti and O-Ti-O vibrational modes in accordance with [12]. The authors of [13] defined five main absorption bands in the IR spectra of MnTiO<sub>3</sub>, namely, 252, 330, 438, 538 and 720 cm<sup>-1</sup>. All these bands were ascribed to Ti-O excitations, but the authors also note that two bands at 252 and 538 cm<sup>-1</sup> can be conditioned by the influence of manganese ions on Ti-O binding.

In the IR absorption spectra of synthesized TMO samples we observed slight broadening and shift of the main absorption bands typical for some components of complex oxides (Fig. 1). Such broadening and complex nature of absorption bands as well as the appearance of new absorption bands in the spectrum is explained by multi-phase nature of TMO particles with almost the same content of manganese ions (13-16% at) but with different ratios of TiO<sub>2</sub>, Mn<sub>2</sub>O<sub>3</sub> and MnTiO<sub>3</sub> crystalline phases. Change in the band shape can be also the result of the presence of structural defects formed due to phase transformations during thermal treatment of the samples, and the influence of the surface phonons as well.

As seen from Fig. 1, the main absorption bands observed for all TMO samples are at 342, 409, 530 and 667 cm<sup>-1</sup> that correlates well with the corresponding Ti-O modes of crystalline rutile. In the IR spectrum of TMO-1 sample we observed the appearance of new bands at 210, 275 and 475 cm<sup>-1</sup> and decrease in the intensity of rutile band at 409 cm<sup>-1</sup>. The first two bands (210 and 275 cm<sup>-1</sup>) are usually ascribed to the deformation excitations of Mn-O in Mn<sub>2</sub>O<sub>3</sub> structure. The band at 475 cm<sup>-1</sup> can be ascribed to Ti-O-Mn excitations. In the IR spectrum of TMO-2 sample we observed the absorption band at ~ 600 cm<sup>-1</sup> typical for the valence excitations of Mn-O [14]. The IR spectrum of this sample is also characterized by the low-frequency band shift at 530 cm<sup>-1</sup> to 10 cm<sup>-1</sup> due to the influence of Mn ions on the excitations of rutile crystalline grating. In the case of TMO the main IR absorption bands of Mn oxides essentially overlap with TiO<sub>2</sub> absorption bands that complicates their assignment. Moreover, identification of absorption bands in the IR spectra of TMO samples is rather complicated due to close location of the characteristic absorption bands of Mn<sub>2</sub>O<sub>3</sub> and MnTiO<sub>3</sub> phases. Thus, presence of MnTiO<sub>3</sub> in TMO-2 and TMO-3 samples is displayed in the IR spectra only as the redistribution of component intensity of the wide absorption band at 600-750 cm<sup>-1</sup>.

### 3.3 CLD spectroscopy

In complex oxide systems the CLD spectra are tightly bound with structure defects that is exhibited in the shift and broadening of some spectral bands. Thus, it was shown in [9] that the changes observed by the authors in CLD spectra of  $\text{TiO}_2$  are connected with the stoichiometric ratio between oxygen and titanium, but not with the particle size.

CLD spectra of An/Mn, R/Mn and TMO powders were studied at room temperature (Fig. 2). In R/Mn spectra (Fig. 2a) three active modes at 144, 446 and 612  $\text{cm}^{-1}$  were observed. In accordance with [15, 16] these fundamental phonons belong to  $B_{1g}$ ,  $E_g$  and  $A_{1g}$  modes of rutile, respectively. CLD-active mode of  $B_{2g}$  symmetry with the maximum of 822  $\text{cm}^{-1}$  is weakly displayed due to its low intensity. Wide band at 235  $\text{cm}^{-1}$  is ascribed to the second-order spectrum. In CLD spectra of TMO samples one can observe the strengthening of the second-order scattering and appearance of a wide background that can be conditioned by the disorder of TMO materials. We have to note that in the CLD spectrum of R/Mn sample we observed the anatase band at 144  $\text{cm}^{-1}$  that is connected with partial phase transformation of anatase to rutile at 900 °C (Table 1).

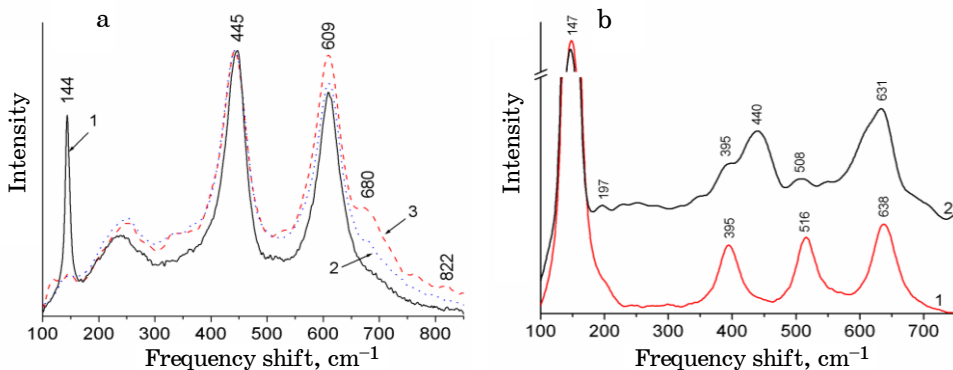


**Fig. 2 – CLD spectra of the samples: a) R/Mn (1), TMO-2 (2), and TMO-3 (3); b) An/Mn (1) and TMO-1 (2)**

Main bands in the CLD spectra of An/Mn sample (Fig. 2b) can be ascribed to the CLD-active modes of crystalline anatase: 147  $\text{cm}^{-1}$  ( $E_g$ ), 197  $\text{cm}^{-1}$  ( $E_g$ ), 395  $\text{cm}^{-1}$  ( $B_{1g}$ ), 516  $\text{cm}^{-1}$  ( $A_{1g}$  and  $B_{1g}$  modes, which can not be separated at room temperature) and 638  $\text{cm}^{-1}$  ( $E_g$ ). All these bands are well observed in the CLD spectrum of TMO-1 sample (Fig. 2b).

Strong CLD band at 651  $\text{cm}^{-1}$  is typical for  $\text{Mn}_2\text{O}_3$  oxide [17, 18]. However we observed this band only for TMO-1 sample while for other samples this band overlaps with  $\text{MnTiO}_3$  (685  $\text{cm}^{-1}$ ) and rutile  $A_{1g}$  (612  $\text{cm}^{-1}$ ) bands. As seen from Fig. 2b, in the CLD spectrum of TMO-1 sample phonon modes both of anatase and rutile are observed. Presence of  $\text{Mn}_2\text{O}_3$  in this sample leads to significant decrease in the intensity of  $B_{1g}$  band at 516  $\text{cm}^{-1}$ . CLD bands of  $\text{Mn}_2\text{O}_3$  oxide at 197  $\text{cm}^{-1}$  and 651  $\text{cm}^{-1}$  [18] overlap with  $E_g$  bands of anatase at 197  $\text{cm}^{-1}$  and 638  $\text{cm}^{-1}$ . In comparison with the CLD spectrum of pure anatase, increase in the background intensity in the spectrum of

TMO-1 sample can be connected with the increase in the second-order scattering due to formation of structural defects in TMO samples.

10 CLD-active modes ( $5A_g + 5E_g$ ) are observed in the CLD spectrum of  $MnTiO_3$  [19], and modes at 202, 235, 263, 336, 360, 462, 610, 684  $\text{cm}^{-1}$  are the most intensive among them [20]. Intensive band at 684  $\text{cm}^{-1}$  is the most typical for  $MnTiO_3$ . This band appears due to the valence excitations of  $A_{1g}$  symmetry of  $MnO_6$  octahedron [21]. The band at 680  $\text{cm}^{-1}$  connected with the formation of Ti-O-Mn bindings is well seen in the obtained CLD spectra of TMO-3 sample, which contains about 14% wt of  $MnTiO_3$ . Other lines in the CLD spectra can be ascribed to the low-frequency phonon modes of  $MnTiO_3$  or their combinations.

It was established [9] that in the CLD spectrum of anatase the location of  $E_g$  mode is between 143 and 147  $\text{cm}^{-1}$  and depends on the sample stoichiometry. The phonon mode  $E_g$  of rutile (446  $\text{cm}^{-1}$ ) is ascribed to the plane deformation excitations of O-O bindings [9], and it is sensitive to oxygen vacancies in  $TiO_2$ . Based on the half-width  $\Delta\nu_{1/2}$  of this rutile band (Fig. 3) we determined the stoichiometric ratio for titanium dioxide in TMO samples and showed that its value is less than 2, i.e., a number of oxygen vacancies is more in comparison with pure  $TiO_2$ . TMO-1 is the most nonstoichiometric among the synthesized TMO samples.

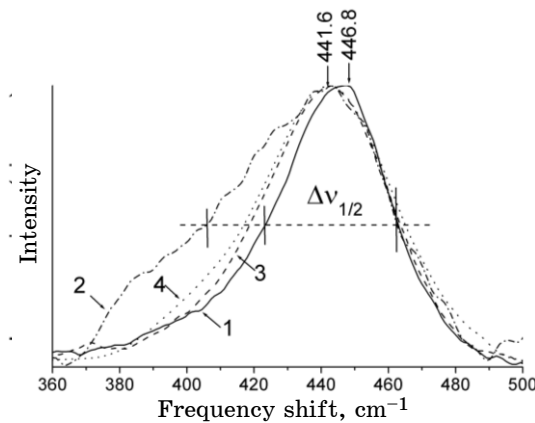


**Fig. 3 –  $E_g$  mode of rutile in CLD spectra of R/Mn (1) and TMO samples: TMO-1 (2), TMO-2 (3), TMO-3 (4)**

### 3.4 Absorption spectra in UV and visible ranges

In Figs. 4 and 5 we present the experimental absorption spectra in UV and visible ranges (2-6 eV) of pure  $TiO_2$  (rutile and anatase) and TMO samples. Obtained absorption spectra have complex nature (Fig. 4) and they can be conditionally divided into three sections.

The first section is the region of photon energies from 2,5 to 3,0 eV. Here one can observe the “tail” of  $TiO_2$  absorption conditioned by the optical transitions between states located nearby the top of the valence band (from 0 to 0,5 eV) and the bottom of the conduction band. As known these states can be connected with bulk structural defects in  $TiO_2$  and can be occupied at room temperature by the thermal excitation of electrons from the valence

band. We assume that essential (4-5 fold) absorption increase in the visible range observed for TMO-2 and TMO-3 samples in comparison with rutile (see Fig. 4) appears due to the overlap of the wide absorption bands of  $\text{MnTiO}_3$  (with maximum  $\nu_{\text{max}} = 2,0\text{-}2,5$  eV) [20] and  $\text{Mn}_2\text{O}_3$  ( $\nu_{\text{max}} = 2,5\text{-}2,75$  eV) [23]. We have also to note the considerable absorption strengthening (about 10-fold) in the TMO-1 spectrum in comparison with pure anatase, and in this case the significant red shift of the absorption edge is observed (Fig. 5). We suppose that the presence of manganese oxides in TMO samples leads to the formation of additional defect states that arouses the increase in absorption intensity.

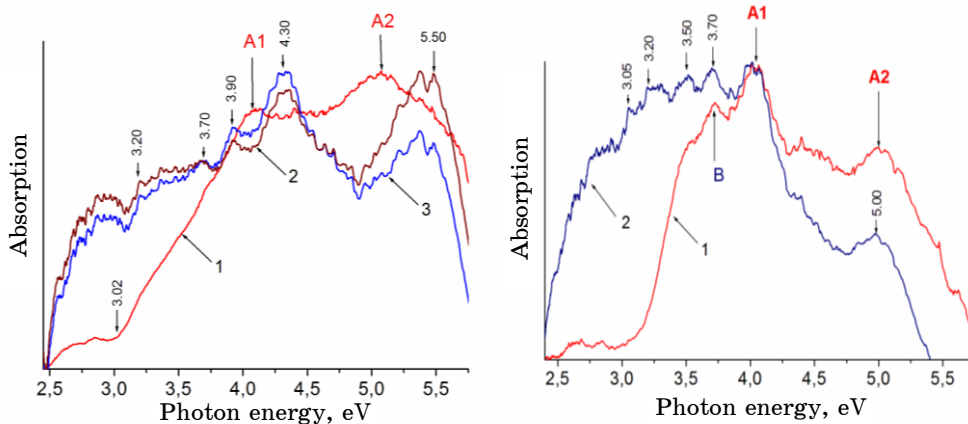


**Fig. 4 – Absorption spectra in UV and visible ranges: R (1), TMO-2 (2) and TMO-3 (3)**

**Fig. 5 – Absorption spectra in UV and visible ranges: An (1) and TMO-1 (2)**

The second section of the absorption spectra is the region of photon energy from 3 to 4 eV. In this spectral section the red shift of the absorption edge more than to 0,5 eV and significant absorption strengthening in comparison with the spectrum of pure rutile are observed for TMO-2 and TMO-3 samples. As a result of the presence of  $\text{Mn}_2\text{O}_3$  and  $\text{MnTiO}_3$  phases in TMO this red shift and absorption increase can be ascribed to the transitions with charge transfer between  $d$ -electrons of Mn and the conduction band of  $\text{TiO}_2$  [24]. For pure anatase (An) and TMO-1 the new absorption maximum (B) is observed at 3,7 eV (Fig.5). This maximum was earlier observed by the authors of [25] for anatase monocrystal at 3,6 eV in the polarization  $\mathbf{E} \perp \mathbf{c}$ . In [26] this maximum was ascribed to the transitions  $\text{O}^{2-} \rightarrow \text{Ti}^{4+}$  with charge transfer. It was also shown that this transition is the dipole-forbidden for the polarization  $\mathbf{E} \parallel \mathbf{c}$  and dipole-allowed for the polarization  $\mathbf{E} \perp \mathbf{c}$ .

The third spectral section covers the region of photon energies from 4,0 to 5,5 eV. In this section two bands with the maximums of  $A_1$  and  $A_2$  are observed in the absorption spectrum of rutile (see Fig. 4). These bands are ascribed to the orbital splitting  $\text{O}2\text{p}_{x,y}$  of oxygen atoms in the valence band [22]. In accordance with [27], the band  $A_1$  at 4,05 eV is connected with the electron transitions between the top of the valence band and the bottom of the conduction band. Another maximum  $A_2$  at 5,08 eV is conditioned by the transitions between four upper valence bands of the valence band and six

bands  $t_{2g}$  of the conduction band. Location of the absorption maximums  $A_1$  and  $A_2$  observed in our work for pure rutile agrees well with location of the absorption maximums of rutile monocrystal observed experimentally in [28] and theoretically calculated in [29]. As well as in the absorption spectrum of rutile, bands  $A_1$  and  $A_2$  in the anatase spectrum (Fig. 5) can be ascribed to the electron transitions from the valence band to  $t_{2g}$  orbitals of the conduction band. In contrast to rutile, in the absorption spectra of anatase intensity of the band  $A_2$  is less than intensity of the peak  $A_1$  ( $I_{A1}/I_{A2} = 1,39$ ).

In comparison with pure rutile, location of the bands  $A_1$  and  $A_2$  for TMO-2 and TMO-3 is shifted to the blue region to 0,2 and 0,3 eV, respectively. In this case the noticeable redistribution of the intensities between the bands  $A_1$  and  $A_2$  is observed. Ratio  $I_{A1}/I_{A2}$  for R : TMO-2 : TMO-3 is changed as 0,86 : 0,92 : 1,27 that can be connected with significant absorption of  $MnTiO_3$  near 300 nm (~ 4 eV) [14, 20]. In the spectrum of TMO-1 location of the bands  $A_1$  and  $A_2$  does not change, but intensity of the band  $A_2$  for this sample is substantially less ( $I_{A1}/I_{A2} = 2,38$ ) than for TMO-2 and TMO-3. Moreover, in the spectrum of TMO-1 sample intensity of absorption bands essentially increases at 3,5 eV and 3,7 eV. Two supplementary bands at 3,25 eV and 3,05 eV are also observed. These bands can be ascribed to the absorption of  $Mn_2O_3$  since absorption of pure rutile and anatase in this region is negligible.

In comparison with the absorption spectrum of pure  $TiO_2$ , the absorption edge in TMO spectra is substantially shifted to the red spectral region that implies about the decrease in the optical band gap width  $E_g$ . It is known [30] that the absorption edge and band gap width of  $TiO_2$  alloyed by Mn depend strongly on the concentration of Mn. Due to strong red shift of the TMO absorption edge we could not determine the exact value of their band gap width within the experimentally studied spectral range since the long-wavelength limit of irradiation of deuterium lamp is about 460 nm.

### 3.5 Photocatalytic decomposition of safranine

To estimate the photocatalytic activity of synthesized  $TiO_2$  and TMO samples we investigated the photocatalytic decomposition of an organic safranine dye ( $C_{20}H_{19}ClN_4$ ) in aqueous solutions under the action of UV irradiation. The obtained results are represented in Table 2 and Fig. 6.

**Table 2 –  $S_{BET}$  for  $TiO_2$  and TMO samples and the velocity constants  $k_d$  under the safranine degradation**

Catalyst	$S_{BET}$ , $m^2/g$	$k_{d1} \times 10^4$ , $s^{-1}$ (30 min)	$k_{d2} \times 10^4$ , $s^{-1}$ (180 min)	$k_{d2}/V$ , $s^{-1}m^{-2}g$
–	–	0,77	0,30	–
An	113	5,82	0,82	0,007
R	15	4,99	1,70	0,113
An/Mn	149	6,14	2,32	0,016
R/Mn	6	4,53	1,63	0,272
TMO-1	13	0,77	0,24	0,018
TMO-2	6	3,53	1,60	0,267

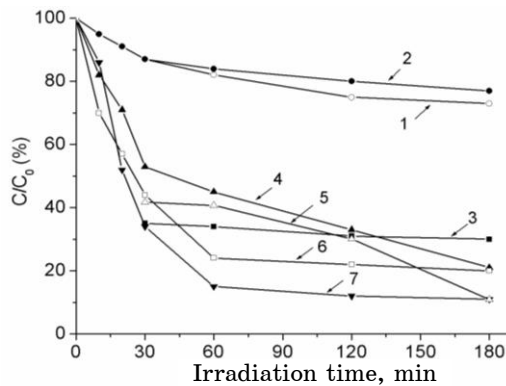
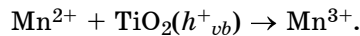


**Fig. 6 – Photocatalytic degradation of safranine without catalyst (1) and with the catalysts: TMO-1 (2), An (3), TMO-2 (4), R (5), R/Mn (6), An/Mn (7)**

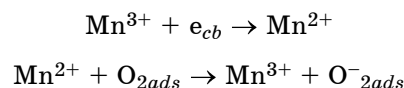
In the absence of catalyst safranine is decomposed very slowly under the action of UV light with the changeless velocity constant  $k_d = 0,3 \cdot 10^{-4} \text{ c}^{-1}$ . In the presence of all catalysts we have studied (except of TMO-1 sample) decomposition velocity of safranine during the first 30 min was the greatest, under the further irradiation the reaction rate decreased. In the case of pure anatase the reaction rate after 30 min substantially decreased that could be connected with deactivation of active centers of anatase surface due to the adsorption of the safranine decay products. Absence of catalytic activity of TMO-1 sample can be conditioned by its phase composition, smaller degree of crystallinity and weak absorption in the region of maximum irradiation of mercury lamp (4,88 eV) (Fig. 5).

In accordance with the results of the CLD spectroscopy, TMO-1 has the most disordered structure and the largest quantity of structural defects, which can be the recombination centers of electron-hole pairs.

The highest photocatalytic activity was shown by the samples of modified by Mn titanium dioxide (R/Mn and An/Mn, Fig. 6) that is connected with the presence of  $\text{Mn}^{2+}$  cations on the surface of  $\text{TiO}_2$  particles. During the UV irradiation the adsorbed  $\text{Mn}^{2+}$  cations can be oxidized at the expense of holes of the semiconductor valence band:



$\text{Mn}^{3+}$  cations formed on the photocatalyst surface are the acceptors or traps for the excited electrons of  $\text{TiO}_2$  conduction band. Thus,  $\text{Mn}^{3+}$  ions inhibit the process of electron and hole recombination. Moreover, electrons trapped by the active centers of  $\text{Mn}^{3+}$  can transit to the adsorbed oxygen  $\text{O}_2$  that also prevents the electron and hole recombination:



Adsorbed oxygen molecules are transformed to the reaction-active superoxide anion radical of oxygen  $\text{O}_{2}^-$ . Moreover, while the photoinduced holes are trapped by surface hydroxyl groups, the photoactive hydroxyl radicals  $\text{HO}$  are formed. Thus, effective spatial separation of photogenerated electrons

and holes occurs. However, when the content of impurity Mn in titanium dioxide increases,  $Mn^{n+}$  cations can be transformed to the centers of electron and hole recombination, and as a result the photoactivity of such samples decreases. Besides, impurity atoms in high concentration on the surface of semiconductor particles can generate the effect of filtration or reflection of UV irradiation that slows down the photoreaction rate.

For the studied samples, the reaction rate of photocatalytic safranine decomposition during the first 30 min of irradiation decreased as An/Mn : An : R : R/Mn : TMO-2 (Table 2). After next 60 min of UV irradiation the greatest degree of safranine decomposition was registered for the samples An/Mn and R/Mn (85% and 75%, respectively). In the presence of TMO-2 the safranine decomposition was 80% during 180 min of the process. High photocatalytic activity of these samples can be explained by the features of their phase composition, high degree of crystallinity (less defective structure), optimal content of Mn ions and strong light absorption in the studied UV range. All these factors lead to the decrease in the contribution of the electron and hole recombination in photocatalysis process and to the increase in the reactivity of the investigated titanium-manganese oxides.

#### 4. CONCLUSIONS

In this work we present the investigation results of the optical and photocatalytic properties of synthesized titanium-manganese mixed oxides (TMO) with different Mn content (13-16% at.). TMO samples were synthesized by the method of chemical precipitation of manganese hydroxide on the polycrystalline particles of pure  $TiO_2$  (rutile or anatase) with further thermal treatment at the temperatures of 300, 850, 900, and 1000 °C. Pure samples of rutile and anatase as well as  $Mn^{2+}$ -doped anatase and rutile were investigated for the comparison.

It is shown that synthesized mixed oxides are the polydisperse materials and contain crystalline phases  $TiO_2$ ,  $Mn_2O_3$  and  $MnTiO_3$ . Absorption spectra in UV and visible range imply that  $Mn_2O_3$ ;  $MnTiO_3$  presence leads to the absorption strengthening nearby the absorption edge (2,5-3,0 eV) and substantial red shift of the absorption edge (on ~ 0,5 eV).

Photocatalytic activity of all synthesized samples in the photodecomposition reaction of an organic safranine dye under the action of UV irradiation is studied. It is shown, that a great amount of structural defects and weak absorption in UV range nearby the irradiation maximum of mercury lamp (4,88 eV) can explain low photoactivity of TMO sample synthesized based on anatase (TMO-1). At the same time, we have registered high photoactivity of anatase and rutile samples with the surface modified by  $Mn^{2+}$  ions as well as TMO sample synthesized based on rutile (TMO-2). We have concluded that mixed titanium-manganese oxides can be the promising photocatalysts in decomposition reactions of organic impurities in aqueous solutions under the action of UV and visible light.

The present work has been performed under the program of NASU “Nanophysics and nanoelectronics” (project No VTs-138).

## REFERENCES

1. A. Fujishima, X. Zhang, D.A. Tryk, *Surf. Sci. Rep.* **63**, 515 (2008).
2. O. Carp, C.L. Huisman, A. Reller, *Prog. Solid. State Ch.* **32**, 33 (2004).
3. D. Chatterjee, S. Dasgupta, *J. Photoch. Photobio. C* **6**, 186 (2005).
4. T. Lopez, P. Bosch, F. Tzompantzi, R. Gomez, J. Navarrete, E. Lopez-Salinas, M.E. Llanos, *Appl. Catal. A-Gen.* **197**, 107 (2000).
5. B. Pal, M. Sharon, G. Nogami, *Mater. Chem. Phys.* **59**, 254 (1999).
6. J. Fang, X. Bi, D. Si, Z. Jiang, W. Huang, *Appl. Surf. Sci.* **253**, 8952 (2007).
7. L. Kernazhitsky, V. Shymanovska, V. Naumov, V. Chernyak, T. Khalyavka, V. Kshnyakin, *Ukr. J. Phys. Opt.* **9**, 197 (2008).
8. V. Shymanovska, A. Dvernyakova, V. Strelko, *Izv. AN SSSR. Neorgan. materialy* **24**, 1188 (1988).
9. J. Parker, R. Siegel, *Appl. Phys. Lett.* **57**, 943 (1990).
10. M. Grujic-Brojcin, M.J. Scepanovic, Z.D. Dohcevic-Mitrovic, I. Hinic, B. Matovic, G. Stasic, Z.V. Popovic, *J. Phys. D: Appl. Phys.* **38**, 1415 (2005).
11. Z.W. Chen, J.K.L. Lai, C.H. Shek, *J. Non-Cryst. Solids.* **352**, 3285 (2006).
12. Y.K. Sharma, M.K. Kharkwal, S. Uma, R. Nagarajan, *Polyhedron* **28**, 579 (2009).
13. Z.Q. Song, S.B. Wang, W. Yang, M. Li, H. Wang, H. Yan, *Mater. Sci. Eng. B* **113**, 121 (2004).
14. F. Pagnanelli, C. Sambenedetto, G. Furlani, F. Vegli‘o, L. Toroa, *J. Power Sources* **166**, 567 (2008).
15. S.P.S. Porto, P.A. Fleury, T.C. Damen, *Phys. Rev.* **154**, 522 (1967).
16. W.S. Li, Z.X. Shen, H.Y. Li, D.Z. Shen, X.W. Fan *J. Raman Spectrosc.* **32**, 862 (2001).
17. G. Busca, *Phys. Chem. Chem. Phys.* **1**, 723 (1999).
18. Z. Chen, S. Tan, S. Zhang, J. Wang, S. Jin, Y. Zhang, H. Sekine, *Jpn. J. Appl. Phys.* **39**, 6293 (2000).
19. R.L. Carter, *Molecular Symmetry and Group Theory* (N-Y: John Wiley & Sons: 1998).
20. G.W. Zhou, Y.S. Kang, *Mater. Sci. Eng.* **24**, 71 (2004).
21. M.I. Baraton, G. Busca, M.C. Prieto, G. Ricchiardi, V.S. Escrivano *J. Solid State Chem.* **112**, 9 (1994).
22. J. Pascual, J. Camassel, H. Mathieu, *Phys. Rev. B* **18**, 5606 (1978).
23. L. Lamaita, M.A. Peluso, J.E. Sambeth, H. Thomas, G. Mineli, P. Porta, *Catal. Today* **107-108**, 133 (2005).
24. W. Choi, A. Termin, M.R. Hoffman, *J. Phys. Chem-US.* **98**, 13669 (1994).
25. N. Hosaka, T. Sekiya, C. Satoko, S. Kurita, *J. Phys. Soc. Jpn.* **66**, 515 (1997).
26. R. Asahi, Y. Taga, W. Mannstadt, A. Freeman, *Phys. Rev. B* **61**, 7459 (2000).
27. K.M. Glassford, J.R. Chelikowsky, *Phys. Rev. B* **46**, 1284 (1992).
28. M. Cardona, G. Harbeke, *Phys. Rev.* **137**, 1467 (1965).
29. F.M. Hossain, L. Sheppard, J. Nowotny, G.E. Murch, *J. Phys. Chem. Solids* **69**, 1820 (2008).
30. W.B. Mi, E.Y. Jiang, H.L. Bai, *Acta. Mater.* **56**, 3511 (2008).
31. S.X. Wu, Z. Ma, Y.N. Qin, X.Z. Qi, Z.C. Liang, *Acta. Phys-Chim. Sin.* **20**, 138 (2004).
32. Y.H. Xu, H.R. Chen, Z.X. Zeng, B. Lei, *Appl. Surf. Sci.* **252**, 8565 (2006).